Part C3 - State of the Solar Photosphere from Spectral Measurements

Franc Rozman

Abstract

Part C2 introduced a differential spectroscopic method that distinguishes between the spatial wavelength of incoming astronomical radiation and the interaction frequency presented to an optical element. Part C3 applies this interpretation to existing solar photospheric measurements and examines whether the resulting plasma velocities are physically compatible with the strong visible luminosity of the photosphere.

The analysis begins with center-to-limb spectral shifts. Within the present model, longitudinal source motion primarily changes interaction frequency, whereas transverse motion changes spatial wavelength according to

$$\frac{\Delta\lambda_{\perp}}{\lambda_0} \approx \frac{v_{\perp}^2}{2c^2}$$

When existing center-to-limb wavelength changes are interpreted through this relation, several independent photospheric spectral lines lead to a characteristic collective velocity scale of approximately

$$v_{\mathrm{plasma}} \sim 300 - 400\ \mathrm{km\,s^{-1}}$$

The result is consistent across different atomic species and is further connected to the distinction between Fabry–Pérot and diffraction-grating measurements developed in Part VIII.

The second part of the paper examines the physical consequences of this velocity range. Collective plasma motion is separated from microscopic thermal motion through

$$v_i = U + \delta v_i$$

so that large bulk velocities do not directly imply extreme thermodynamic temperatures. Because of the small electron mass, electron kinetic energies associated with velocities of 300–400 km/s remain of order 0.3–0.5 eV. Such electrons can participate in capture, recombination, excitation, and radiative cascades, while the much larger collective kinetic-energy reservoir of the plasma can drive turbulence, mixing, ionization, and repeated particle exchange.

The visible radiative power is therefore interpreted primarily through the rate of microscopic events,

$$P_{\mathrm{vis}} \sim R_{\mathrm{events}}\overline{E_{\gamma}}$$

rather than through one unique electron energy. Large collective velocities are important because they can strongly increase plasma dynamics and the frequency of radiative interactions.

The central result is that two independent lines of reasoning converge on the same velocity scale: spectral measurements interpreted through the Part C2 model indicate collective velocities of several hundred kilometres per second, while velocities in this range also provide a favorable dynamical regime for sustaining intense visible photospheric radiation. The measurement interpretation and the proposed physical model of the photosphere are therefore mutually consistent within the present framework.

.

1. Introduction

Solar spectroscopy provides some of the most precise measurements available in astrophysics. Spectral-line positions, line widths, bisectors, and their variation across the solar disk are routinely converted into velocities of the photospheric plasma. The precision of the measurement, however, does not by itself determine whether the physical interpretation assigned to that measurement is unique.

Part C2 introduced a distinction between the spatial wavelength of incident radiation and the frequency with which the electromagnetic structure interacts with a moving observer or optical element. Within that model, a Fabry–Pérot interferometer and a diffraction grating need not provide equivalent representations of the same source motion. The present paper examines the consequences of this distinction for existing solar observations.

The first question is observational:

What plasma velocities follow if the measured center-to-limb wavelength changes are interpreted through the measurement principles developed in Part C2?

In the present model, longitudinal and transverse motion of the source affect the electromagnetic structure differently. Longitudinal motion changes the interaction frequency, while transverse motion changes the spatial wavelength.

The distinction may be written schematically as

$$v_{\parallel} \rightarrow \Delta f$$

and

$$v_{\perp} \rightarrow \Delta\lambda$$

A wavelength displacement measured by a Fabry–Pérot interferometer therefore need not represent the full longitudinal velocity of the source.

This becomes particularly important for the solar photosphere. Near the center of the solar disk, locally vertical plasma motion is predominantly longitudinal relative to the observer. Toward the limb, the same physical motion becomes increasingly transverse.

The solar disk therefore provides a natural geometrical transformation:

$$\text{longitudinal motion at disk center} \rightarrow \text{increasingly transverse motion toward the limb}$$

Within the present model, the observed center-to-limb redward displacement can consequently contain information about the magnitude of the underlying collective plasma velocity.

Existing measurements of several photospheric spectral lines show systematic center-to-limb

wavelength changes of only a few hundred metres per second when expressed through the conventional Doppler relation. When interpreted instead as a transverse-wavelength effect, these small spectral changes correspond to characteristic collective plasma velocities of the order of

$$v_{\mathrm{plasma}} \sim 300 - 400\ \mathrm{km\,s^{-1}}$$

The difference is therefore not a small numerical correction. It represents a fundamentally different physical interpretation of the same measured spectral displacement.

The first part of this paper develops this argument from the measurement itself. It examines what a Fabry–Pérot interferometer actually measures, how longitudinal and transverse source motion are separated, how the center-to-limb geometry transforms the observed velocity components, and whether different spectral lines lead to a consistent characteristic velocity scale. The comparison with diffraction-grating spectroscopy is then used to connect these results directly with the experimental principle developed in Part C2.

The second question is physical:

Are collective plasma velocities of several hundred kilometres per second compatible with the strong visible radiation of the photosphere?

At first sight, such velocities may appear extremely large compared with the conventional photospheric velocity scale. Their physical meaning, however, depends critically on whether they represent random thermal motion or organized collective plasma motion.

The velocity of a particle can be written as

$$v_i = U + \delta v_i$$

where U is the collective velocity of the plasma flow and δv_i is the particle velocity relative to that flow.

A large value of $mathbfU$ does not by itself imply a high thermodynamic temperature.

This distinction is especially important for electrons. Because of their small mass, an electron moving at several hundred kilometres per second carries only a small kinetic energy.

For example,

$$v_e = 300\ \mathrm{km\,s^{-1}} \Rightarrow E_{k,e} \approx 0.26\ \mathrm{eV}$$

and

$$v_e = 400\ \mathrm{km\,s^{-1}} \Rightarrow E_{k,e} \approx 0.46\ \mathrm{eV}$$

Such energies are entirely different from the energies of electrons in the high-energy tail of a hot plasma.

Low-energy electrons can enter the Coulomb fields of ions, become captured when energy is transferred away, and subsequently participate in radiative cascades. Visible photons can therefore be produced even when the kinetic energy of the incoming electron is less than one electronvolt, because the emitted radiation can also include the binding energy released during capture.

The production of visible radiation is consequently not restricted to one narrow electron-energy range.

Large collective plasma velocities are important for a different reason.

Neighboring plasma flows with different velocities create shear, turbulence, mixing, electromagnetic fluctuations, and repeated exchange of particles between different local environments. These processes increase the number of ionization, capture, excitation, recombination, and radiative-transition events.

The visible luminosity can therefore be represented schematically as

$$P_{\mathrm{vis}} \sim R_{\mathrm{events}}\overline{E_\gamma}$$

where R_{events} is the total rate of visible-light-producing microscopic processes.

A large radiative power does not require an exceptionally large energy per event if the event rate is enormous.

This provides the central connection developed in the present paper.

The spectral interpretation leads to a characteristic collective velocity scale of several hundred kilometres per second. The same velocity scale implies a strongly dynamic photosphere in which plasma flows interact, mix, exchange electrons, and continuously regenerate the microscopic conditions required for strong visible radiation.

The central argument can therefore be summarized as two connected sequences:

$$\text{spectral measurement} \rightarrow \text{transverse interpretation} \rightarrow 300 - 400\ \text{km s}^{-1}$$

and

$$300 - 400\ \text{km s}^{-1} \rightarrow \text{strong plasma dynamics} \rightarrow \text{high microscopic event rate} \rightarrow \text{strong visible radiation}$$

The purpose of Part IX is to examine whether these two independent lines of reasoning converge on the same physical picture of the solar photosphere.

2. What the Spectral Measurement Actually Provides

Spectroscopic instruments do not measure plasma velocity directly. They respond to properties of the electromagnetic field reaching the instrument. Velocity is introduced only after the measured optical quantity is interpreted through a model relating source motion, frequency, wavelength, and instrument response.

This distinction is essential for the present paper.

A spectral measurement therefore contains two separate steps:

$$\text{optical measurement} \rightarrow \text{physical interpretation}$$

The first step is experimental. The second is model-dependent.

For the present discussion, the central question is not simply

What velocity does the instrument report?

but rather

What optical quantity did the instrument measure before that quantity was converted into velocity?

2.1 Fabry–Pérot Interferometer

A Fabry–Pérot interferometer responds to the phase condition established between repeated reflections inside the optical cavity.

For normal incidence, the resonance condition is

$$2nL = m\lambda$$

where n is the refractive index inside the cavity, L is the mirror separation, m is the interference order, and λ is the spatial wavelength inside the cavity.

The directly observed quantity is therefore the transmission condition produced by the spatial phase structure of the incoming radiation.

The FPI does not directly measure source velocity.

Velocity is inferred only later, usually by comparing the measured wavelength with a reference wavelength.

The conventional small-velocity Doppler conversion is

$$v_{\text{LOS}} = c\frac{\Delta\lambda}{\lambda_0}$$

This relation assigns a line-of-sight velocity to the observed wavelength displacement.

Within the present model, however, this conversion is not automatically equivalent to a direct velocity measurement.

If longitudinal source motion changes the interaction frequency without producing the corresponding spatial-wavelength change, then the FPI responds primarily to

$$\lambda$$

rather than directly to

$$v_{\parallel}$$

The experimentally measured quantity must therefore be kept separate from the velocity assigned to it.

2.2 Frequency and Wavelength Must Be Separated

In conventional wave descriptions, frequency and wavelength are commonly connected through

$$u = f\lambda$$

The present model retains this relation but allows u, f, andλ to respond differently to source motion.

This makes the distinction between frequency and spatial wavelength physically important.

For purely longitudinal source motion, the present model assumes that the emitted spatial wavelength remains approximately unchanged:

$$\lambda_{\parallel} = \lambda_0$$

while the interaction frequency changes.

For transverse motion, the frequency can remain unchanged while the geometrical propagation path and spatial wavelength increase.

Thus, a measured wavelength displacement does not uniquely identify which component of source motion produced it.

2.3 Measured Wavelength Is Not Yet a Velocity

Suppose an FPI measures a displacement

$$\Delta\lambda = \lambda - \lambda_0$$

The experimental result is the wavelength displacement itself.

Only after applying an interpretive relation does one obtain a velocity.

Conventionally,

$$\Delta\lambda \rightarrow v_{\mathrm{LOS}}$$

Within the present model, however, the same measured $\Delta\lambda$ may contain a substantial transverse-motion contribution.

The measurement chain should therefore be written as

$$\begin{aligned}\text{source motion} &\rightarrow \text{electromagnetic structure}\\ &\rightarrow \text{instrument response}\\ &\rightarrow \Delta\lambda\\ &\rightarrow \text{velocity interpretation}\end{aligned}$$

The final arrow is not part of the optical measurement itself.

2.4 Diffraction Grating

A diffraction grating presents a different measurement problem.

Conventionally, for normal incidence,

$$d\sin\theta_m = m$$

where d is the grating spacing and θ_m is the diffraction angle of order m.

Experimentally, the detector records the position or angle at which the radiation emerges. Wavelength is then assigned through the calibrated grating geometry.

Within the present model, the grating has an additional role.

It is treated as an optical element that reconstructs the outgoing electromagnetic wave. The frequency presented to the grating can therefore determine the wavelength of the reconstructed radiation.

The measurement chain becomes

$$\begin{aligned}\text{incoming field} &\rightarrow \text{grating interaction}\\ &\rightarrow \text{reconstructed wave}\\ &\rightarrow \text{diffraction angle} \rightarrow\end{aligned}$$

This is fundamentally different from assuming that the grating merely sorts an already fixed incident wavelength.

2.5 Why FPI and Grating Measurements Need Not Be Equivalent

This distinction becomes important when the source contains a broad distribution of longitudinal velocities.

Within the present model, an FPI can retain a relatively narrow spatial-wavelength structure even when the longitudinal velocity distribution is large.

A diffraction grating, however, can convert the corresponding interaction-frequency distribution into a broad reconstructed wavelength distribution.

Schematically,

$$\text{FPI} \rightarrow \text{direct response to spatial wavelength}$$

while

$$\text{grating} \rightarrow \text{reconstruction of wavelength from interaction frequency}$$

The two instruments can therefore respond differently to the same rapidly moving plasma.

This is the central experimental distinction developed in Part VIII.

2.6 The Relevant Quantity for Solar Measurements

For the solar photosphere, the practical consequence is straightforward.

A measured spectral displacement should first be treated as an optical result:

$$\Delta\lambda_{\text{measured}}$$

before it is interpreted as a plasma velocity.

The present paper therefore does not begin by assuming that

$$\Delta\lambda_{\text{measured}} = \Delta\lambda_{\text{longitudinal}}$$

Instead, it asks whether part of the observed wavelength change can arise from transverse collective plasma motion.

This question becomes especially useful across the solar disk because the same local plasma motion changes continuously from predominantly longitudinal near disk center to increasingly transverse toward the limb.

The center-to-limb geometry therefore provides a natural test of the distinction between

$$\Delta f$$

and

$$\Delta\lambda$$

developed in Part VIII.

The next section examines how longitudinal and transverse source motion are represented separately in the present model.

3. Longitudinal and Transverse Motion

The interpretation of solar spectral measurements depends critically on how the source velocity is divided into longitudinal and transverse components relative to the observer.

Let the source velocity be

$$v = v_{\parallel} + v_{\perp}$$

with

$$v^2 = v_{\parallel}^2 + v_{\perp}^2$$

where $v_{\parallel}$ is the component parallel to the line of sight and $v_{\perp}$ is the component perpendicular to it.

Within the present model, these two components do not affect the observed electromagnetic structure in the same way.

3.1 Longitudinal Motion

For longitudinal source motion, the emitted spatial wavelength is taken to remain unchanged after emission:

$$\lambda_{\parallel} = \lambda_0$$

while the interaction frequency changes with the relative longitudinal velocity.

For motion toward the observer,

$$f_{\parallel} = f_0 \left(1 + \frac{v_{\parallel}}{c}\right)$$

and for motion away from the observer,

$$f_{\parallel} = f_0 \left(1 - \frac{v_{\parallel}}{c}\right)$$

for

$$\left|v_{\parallel}\right| \ll c$$

The important distinction is therefore

$$\Delta f_{\parallel} \neq 0$$

while

$$\Delta\lambda_{\parallel} = 0$$

for purely longitudinal motion in the present interpretation.

A large radial source velocity can therefore alter the frequency with which successive electromagnetic structures interact with the observer without producing the corresponding change in their spatial wavelength.

This distinction is central to the interpretation of Fabry–Pérot measurements.

3.2 Transverse Motion

For transverse source motion, the situation is different.

If the source moves perpendicular to the line of sight during one emission period T, the source changes its transverse position by

$$v_{\perp} T$$

while the electromagnetic structure propagates a distance

cT

in the longitudinal direction.

The corresponding geometrical propagation distance is therefore

$$uT = \sqrt{(cT)^2 + (v_{\perp}T)^2}$$

and hence

$$u = \sqrt{c^2 + v_{\perp}^2}$$

The emission frequency remains unchanged:

$$f_{\perp} = f_0$$

Since

$$\lambda_0 = cT$$

and

$$\lambda_{\perp} = uT$$

the transverse wavelength becomes

$$\lambda_{\perp} = \lambda_0 \sqrt{1 + \frac{v_{\perp}^2}{c^2}}$$

Thus, transverse source motion increases the spatial wavelength.

For

$$v_{\perp} \ll c$$

the square root can be expanded:

$$\sqrt{1 + \frac{v_{\perp}^2}{c^2}} \approx 1 + \frac{v_{\perp}^2}{2c^2}$$

and therefore

$$\frac{\Delta\lambda_{\perp}}{\lambda_0} \approx \frac{v_{\perp}^2}{2c^2}$$

This contribution is always positive.

Within the present model, transverse motion therefore produces a redward wavelength displacement independent of the sign of the transverse velocity.

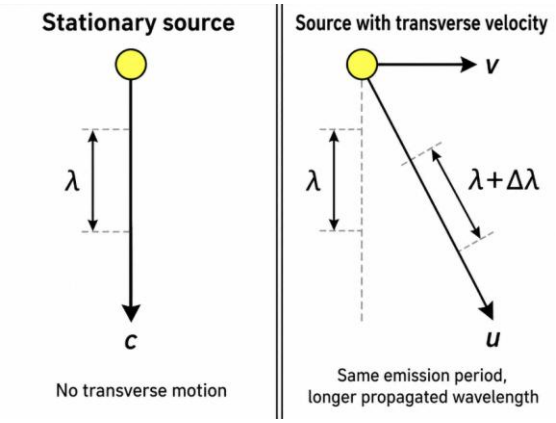

***Figure 1**. Geometrical origin of the transverse wavelength increase in the present model. For a stationary source, the distance propagated during one emission period T is $\lambda_0 = cT$. If the source moves transversely with velocity v, the corresponding propagation path becomes uT, where $u^2 = c^2 + v^2$. The emission frequency remains unchanged, while the spatial wavelength increases to $\lambda_\perp = uT = \lambda_0\sqrt{1+v^2/c^2}$.*

3.3 Apparent Doppler Velocity

If the transverse wavelength increase is interpreted using the conventional first-order Doppler relation,

$$V_{\mathrm{app}} = c\frac{\Delta\lambda}{\lambda_0}$$

then substitution gives

$$V_{\mathrm{app}} \approx \frac{v_\perp^2}{2c}$$

and therefore

$$v_\perp \approx \sqrt{2cV_{\mathrm{app}}}$$

This relation is important because a small apparent Doppler velocity can correspond to a much larger transverse collective velocity.

For example, if

$$V_{\mathrm{app}} = 200\ \mathrm{m\,s^{-1}}$$

then

$$v_\perp \approx \sqrt{2cV_{\mathrm{app}}}$$

gives a transverse velocity of several hundred kilometres per second.

The difference between the apparent spectroscopic velocity and the inferred physical velocity can therefore be very large.

3.4 Combined Motion

For a general plasma trajectory, both components can be present simultaneously.

Within the present model,

$$v_\parallel \rightarrow \Delta f$$

while

$$v_\perp \rightarrow \Delta\lambda$$

The two effects should therefore be kept conceptually separate.

A spectroscopic instrument that responds primarily to spatial wavelength can be much more sensitive to the transverse component than to the longitudinal component of the same physical plasma motion.

3.5 Application to the Solar Disk

The solar photosphere provides a particularly useful geometry for separating these effects.

Near disk center, locally vertical plasma motion is predominantly longitudinal relative to the observer.

Toward the limb, the same local vertical motion becomes increasingly transverse.

The plasma velocity itself does not need to change.

What changes is its decomposition relative to the observer:

$$\text{disk center} \rightarrow v_\parallel \text{ dominant}$$

and

$$\text{toward limb} \rightarrow v_\perp \text{ increasingly important}$$

Within the present model, the increasing transverse component produces an increasing redward wavelength contribution.

The observed center-to-limb spectral shift can therefore be used to estimate the underlying collective plasma velocity.

The next section develops this relation quantitatively from existing solar measurements.

4. Center-to-Limb Measurements and the Inferred Plasma Velocity

The solar disk provides a natural geometrical test of the distinction developed in the previous section. A plasma flow that is locally vertical is viewed almost longitudinally at disk center and increasingly transversely toward the limb.

Let

$$\mu = \cos\theta$$

where θ is the heliocentric angle. Thus,

$$\mu = 1$$

at disk center and

$$\mu \to 0$$

toward the limb.

If the observed center-to-limb wavelength displacement contains a transverse-motion contribution, the changing viewing geometry allows the characteristic plasma velocity to be estimated.

4.1 Vertical and Horizontal Velocity Components

Let the mean-square vertical velocity component be written as

$$\sigma_z^2 = \overline{v_z^2}$$

and let the two horizontal components satisfy

$$\sigma_h^2 = \overline{v_x^2} = \overline{v_y^2}$$

For an azimuthally symmetric distribution of horizontal motion, the mean-square velocity perpendicular to the line of sight is

$$\overline{v_\perp^2} = \sigma_h^2(1+\mu^2) + \sigma_z^2(1-\mu^2)$$

Within the transverse-wavelength model of Section 3, the corresponding apparent spectroscopic velocity is

$$V_\perp(\mu) = \frac{\sigma_h^2(1+\mu^2) + \sigma_z^2(1-\mu^2)}{2c}$$

At disk center,

$$V_\perp(1) = \frac{\sigma_h^2}{c}$$

while near the limb,

$$V_\perp(0) = \frac{\sigma_h^2 + \sigma_z^2}{2c}$$

The center-to-limb difference is therefore

$$V_\perp(\mu) - V_\perp(1) = \frac{(\sigma_z^2 - \sigma_h^2)(1-\mu^2)}{2c}$$

This relation is especially useful because it depends on the difference between the vertical and horizontal mean-square velocity components.

4.2 Elimination of Constant Spectral Offsets

A constant wavelength displacement affecting the whole solar disk does not contribute to the center-to-limb difference.

This applies, for example, to any approximately constant gravitational redshift term.

If

$$V_{\rm obs}(\mu) = V_{\rm const} + V_\perp(\mu)$$

then

$$V_{\rm obs}(\mu) - V_{\rm obs}(1) = V_\perp(\mu) - V_\perp(1)$$

The analysis can therefore use the measured change across the solar disk without requiring the absolute zero point of the spectral line to be known with the same precision.

This is one of the advantages of the center-to-limb comparison.

4.3 Characteristic Anisotropic Velocity

Define

$$D = \sqrt{\sigma_z^2 - \sigma_h^2}$$

The center-to-limb relation then becomes

$$\Delta V_{\mathrm{CL}}(\mu) = \frac{D^2(1-\mu^2)}{2c}$$

and therefore

$$D = \sqrt{\frac{2c\Delta V_{\mathrm{CL}}}{1-\mu^2}}$$

For measurements extending to approximately

$$\mu = 0.3$$

this becomes

$$D = \sqrt{\frac{2c\Delta V_{\mathrm{CL}}}{0.91}}$$

The quantity D does not represent the full three-dimensional plasma velocity. It represents the characteristic difference between the vertical and horizontal velocity scales implied by the center-to-limb signal within the present model.

The quantity D measures the anisotropy between the vertical and horizontal velocity components. It is not, in general, equal to the total plasma velocity. If the photospheric flows are predominantly vertical, so that $\sigma_h \ll \sigma_z$, then $D \approx \sigma_z$ and may be used as an estimate of the characteristic vertical collective-flow velocity.

4.4 Numerical Scale from Existing Measurements

Existing high-precision solar measurements show center-to-limb spectral changes of order only a few hundred metres per second when expressed as conventional apparent Doppler velocities.

Representative changes of approximately

$$\Delta V_{\mathrm{CL}} \sim 130 - 210\ \mathrm{m\,s^{-1}}$$

correspond, through the preceding relation, to

$$D \sim 290 - 370\ \mathrm{km\,s^{-1}}$$

Thus, an observed spectral change of only a few hundred metres per second can correspond, in the transverse interpretation, to a collective plasma velocity scale of several hundred kilometres per second.

The large numerical difference follows from the quadratic relation

$$\Delta V_{\mathrm{CL}} \propto \frac{v_\perp^2}{2c}$$

rather than from the conventional first-order longitudinal relation

$$\Delta V \propto v_\parallel$$

4.5 Physical Meaning of the Result

The inferred quantity should not be interpreted as random thermal velocity.

The analysis instead suggests that the observed center-to-limb shift may contain the signature of organized or partially organized plasma motion with a strong vertical component.

If

$$\sigma_z > \sigma_h$$

then the redward displacement increases toward the limb, as observed in the present interpretation.

This naturally points toward vertically structured flows rather than an isotropic velocity distribution.

The result can therefore be summarized as

$$\text{small center-to-limb spectral shift} \\ \rightarrow \text{large anisotropic collective velocity}$$

with a characteristic scale of approximately

$$300 - 400\ \mathrm{km\,s^{-1}}$$

for the measurements considered here.

4.6 Why the Center-to-Limb Geometry Is Important

The importance of the solar disk is not merely that many spectral measurements are available.

It is that the observing geometry continuously changes the decomposition of the same local motion.

A locally vertical flow contributes mainly to the longitudinal component at disk center:

$$v_{\parallel} \approx v_z$$

while toward the limb it contributes increasingly to the transverse component:

$$v_{\perp} \approx v_z$$

The center-to-limb observation therefore acts as a geometrical transformation of the same underlying plasma motion.

Within the present model, this allows the transverse contribution to be extracted without physically changing the source or the measuring instrument.

4.7 Main Result of the Center-to-Limb Analysis

The central result of this section is that the small observed center-to-limb wavelength changes need not imply plasma velocities of only a few hundred metres per second.

Under the transverse-wavelength interpretation developed in Part VIII and Section 3 of this paper, they correspond to a characteristic anisotropic velocity scale of several hundred kilometres per second.

The next question is whether this result is specific to one spectral line or whether different photospheric lines lead to a similar velocity scale. That comparison is considered in the next section.

5. Consistency Across Different Spectral Lines

The center-to-limb analysis becomes more significant if different photospheric spectral lines lead to the same general velocity scale.

A result obtained from only one line could be strongly influenced by the local formation conditions of that transition, by line asymmetry, or by radiative-transfer effects. If several independent lines formed by different atomic species produce comparable inferred velocities, the interpretation becomes more physically coherent.

The present comparison therefore asks:

Do different spectral lines point to the same characteristic photospheric velocity scale when the observed center-to-limb wavelength changes are interpreted through the transverse-motion relation?

The several lines of Si I, Sc II, Fe I, and Ti I yield the same general scale of a few hundred kilometres per second when analyzed in this way.

5.1 Characteristic Velocity from Each Line

For each spectral line, the procedure is the same.

The measured center-to-limb wavelength change is first expressed as an apparent velocity difference,

$$\Delta V_{\mathrm{CL}}$$

and then converted through

$$D = \sqrt{\frac{2c\Delta V_{\mathrm{CL}}}{1-\mu^2}}$$

where

$$D = \sqrt{\sigma_z^2 - \sigma_h^2}$$

represents the characteristic anisotropic velocity scale.

The resulting values are not expected to be identical because different spectral lines form under different physical conditions and over different height ranges.

The important question is whether they cluster around the same order of magnitude.

5.2 Direct Derivation from Published LARS Measurements

The values used in the present comparison are derived from the published line-core Doppler velocities reported by Löhner-Böttcher et al. (2018) – (4). For each spectral line, the center-to-limb difference is calculated between disk center, $\mu = 1.0$, and $\mu = 0.3$:

$$\Delta V_{\mathrm{CL}} = V(\mu = 0.3) - V(\mu = 1.0)$$

The corresponding anisotropic velocity scale is then obtained from the transverse-motion relation derived in Section 4:

$$D = \sqrt{\frac{2c\Delta V_{\mathrm{CL}}}{1 - 0.3^2}}$$

The first two numerical columns in Table 1 are therefore published observational values. The last two columns are calculated in the present work.

Spectral line	$V(\mu = 1.0)$ [m/s]	V(μ=0.3) m/s	ΔV_{CL} m/s	D km/s
Si I 6299.590 Å	−253	−48	205	368
Sc II 6300.6795 Å	−387	−241	146	310
Fe I 6301.5008 Å	−107	+85	192	356
Fe I 6302.4932 Å	−164	+33	197	360
Fe I 6303.460 Å	−420	−277	143	307
Ti I 6303.7565 Å	−353	−225	128	290

Table 1. *Published line-core Doppler velocities at $\mu = 1.0$ and $\mu = 0.3$ from Löhner-Böttcher et al. (2018) – (4), together with the center-to-limb differences and the values of D calculated in the present work. The values of D are not directly measured plasma velocities. They are inferred from the published center-to-limb wavelength shifts through the transverse-motion relation developed in Section 4*

5.2 Representative Results

The derived values occupy a relatively narrow interval:

$$D \approx 290 - 370\ \mathrm{km\,s^{-1}}$$

The important result is not one particular value, but the repeated appearance of the same characteristic anisotropic velocity scale across several independent spectral lines.

The previously analyzed lines give representative characteristic values approximately in the following range:

Spectral line	Characteristic velocity D
Si I	$\sim 368\ \mathrm{km\,s^{-1}}$
Sc II	$\sim 310\ \mathrm{km\,s^{-1}}$
Fe I 6301.5 Å	$\sim 356\ \mathrm{km\,s^{-1}}$
Fe I 6302.5 Å	$\sim 360\ \mathrm{km\,s^{-1}}$
Fe I 6303.5 Å	$\sim 307\ \mathrm{km\,s^{-1}}$
Ti I	$\sim 290\ \mathrm{km\,s^{-1}}$

Table 2*. Published center-to-limb line-core shifts and derived values of D. Published line-core Doppler velocities at disk center, $\mu = 1.0$, and at $\mu = 0.3$, together with the corresponding center-to-limb difference ΔV_{CL} and the anisotropic velocity scale D calculated in the present work. The observational values are from Löhner-Böttcher et al. (2018); the last two columns are derived using the relation introduced in Section 4.*

The values used here are derived from the line-core Doppler velocities listed in Table 2 of Löhner-Böttcher et al. (2018)- (4). For each spectral line, the center-to-limb difference is taken between $\mu = 1.0$ and \mu=0.3, and then converted to \(D\) using the transverse-motion relation of Section 4

The individual values differ, but they occupy a relatively narrow interval:

$$D \approx 290 - 370\ \mathrm{km\,s^{-1}}$$

The important result is therefore not one particular number but the repeated appearance of the same characteristic scale:

$$D \sim 300 - 400\ \mathrm{km\,s^{-1}}$$

across different spectral lines.

5.3 The Result Is Not Controlled by Atomic Mass

The lines in the comparison arise from different atomic species.

If the inferred velocity scale were simply a consequence of random thermal motion, one would generally expect particle mass to be relevant to the characteristic thermal velocity.

The present interpretation is different.

The similar values obtained from different species suggest that the measured effect may be associated primarily with a common collective plasma motion:

$$v_i = U + \delta v_i$$

where the same collective velocity

$$U$$

is shared approximately by electrons, ions, and neutral particles within the local flow.

The mass of the emitting atom then does not determine the bulk velocity.

This is consistent with the interpretation of the photosphere as a system of organized plasma flows rather than as a collection of independent particles whose measured spectral shifts are determined only by thermal velocity.

5.4 Differences Between Lines Are Still Expected

The agreement should not be interpreted as exact equality.

Different spectral lines are formed over different atmospheric regions and respond differently to temperature, density, ionization, opacity, and radiative transfer.

Their effective velocity sampling may therefore differ.

The characteristic value should more realistically be written as

$$D_i = D(z_i, \rho_i, T_i, \text{line formation})$$

where the index i denotes the spectral line.

The spread between approximately 290 and 370 km/s can therefore contain information about differences in the regions sampled by the individual lines rather than representing an inconsistency of the model.

5.5 Different Fe I Lines

The comparison between several Fe I lines is especially useful because the atomic mass is essentially the same.

Representative values of approximately

$$D \approx 356\ \mathrm{km\,s^{-1}}$$

for Fe I 6301.5 Å,

$$D \approx 360\ \mathrm{km\,s^{-1}}$$

for Fe I 6302.5 Å, and

$$D \approx 307\ \mathrm{km\,s^{-1}}$$

for Fe I 6303.5 Å

cannot be explained by differences in atomic mass.

The differences must instead arise from the particular parts of the photosphere sampled by the lines, from the internal line-formation structure, or from additional radiative-transfer effects.

This supports the idea that the center-to-limb signal contains information about the geometry and dynamics of the line-forming region.

5.6 Different Parts of the Same Spectral Line

The same reasoning applies even within a single spectral line.

The existing analysis of Fe I 6301.5 Å showed that the bisector does not shift rigidly as one structure. Different intensity levels show different center-to-limb wavelength changes.

Within the present interpretation, this suggests that different parts of the line sample regions with different characteristic plasma dynamics.

Thus,

$$D_{\text{core}} \neq D_{\text{wing}}$$

need not indicate a failure of the velocity interpretation.

Instead, it may indicate that the collective velocity field changes with height or with the physical conditions in the line-forming region.

5.7 Main Result

The comparison of different spectral lines therefore gives a simple but important result.

Several independent photospheric lines converge on the same characteristic velocity scale:

$$v_{\text{characteristic}} \sim 300 - 400\ \text{km s}^{-1}$$

while the remaining differences between individual lines are moderate and physically plausible for lines formed in different atmospheric regions.

The consistency across different species is particularly significant because it points toward a common collective plasma motion rather than toward an effect controlled primarily by atomic mass.

The first part of the paper has therefore produced the same velocity scale in more than one way.

The next question is whether Fabry–Pérot and diffraction-grating spectroscopy should reveal this plasma motion in the same form. That distinction is considered in the next section.

6. Fabry–Pérot and Diffraction-Grating Measurements

The velocity scale inferred in the previous sections is much larger than the apparent Doppler velocities usually associated with photospheric line shifts. This raises an immediate experimental question:

If plasma motions of several hundred kilometres per second are present, why do conventional solar spectra not simply display enormously broadened or displaced lines?

Within the present model, the answer depends on the measuring instrument.

The distinction developed in Part VIII is that a Fabry–Pérot interferometer and a diffraction grating need not preserve and display the same property of the incoming electromagnetic field.

6.1 Fabry–Pérot Measurement

A Fabry–Pérot interferometer responds primarily to the spatial wavelength that satisfies its resonance condition,

$$2nL = m\lambda$$

Within the present model, purely longitudinal source motion changes the interaction frequency but does not necessarily change the spatial wavelength of the incoming structure:

$$\Delta f_{\parallel} \neq 0$$

while

$$\Delta\lambda_{\parallel} = 0$$

A broad distribution of longitudinal plasma velocities can therefore remain comparatively inconspicuous in an FPI wavelength measurement.

The FPI can still reveal the transverse contribution discussed in Sections 3 and 4, because transverse motion modifies the spatial wavelength itself.

Thus, within the present interpretation,

$$\text{FPI} \rightarrow \text{primarily spatial-wavelength information}$$

This is why relatively small center-to-limb wavelength displacements can coexist with much larger inferred collective velocities.

6.2 Diffraction Grating

The diffraction grating is treated differently in the present model.

At the grating, the incoming electromagnetic structure is spatially reconstructed. The outgoing wave then propagates relative to the grating with propagation velocity c, while its reconstructed wavelength is determined by the interaction frequency presented to the grating.

Thus,

$$\lambda_{\mathrm{gr}} = \frac{c}{f_{\mathrm{int}}}$$

A distribution of longitudinal source velocities therefore becomes a distribution of reconstructed wavelengths.

Schematically,

$$\begin{aligned}\text{longitudinal velocity distribution} &\rightarrow \text{frequency distribution} \\ &\rightarrow \text{grating reconstruction} \\ &\rightarrow \text{wavelength distribution}\end{aligned}$$

A diffraction grating can therefore reveal a velocity component that is much less visible in the direct Fabry–Pérot wavelength measurement.

6.3 Expected Width for Several Hundred Kilometres per Second

For small velocities, the reconstructed wavelength displacement is approximately

$$\frac{|\Delta\lambda|}{\lambda_0} \approx \frac{|v|}{c}$$

For a representative photospheric wavelength

$$\lambda_0 = 630.15\ \mathrm{nm}$$

and a velocity magnitude

$$|v| = 400\ \mathrm{km\,s^{-1}}$$

the displacement on one side of the distribution is approximately

$$|\Delta\lambda| \approx 0.84\ \mathrm{nm}$$

A symmetric velocity range from approximately -400 to +400 $\mathrm{km\,s^{-1}}$ would therefore correspond to a reconstructed spectral width of roughly

$$W \approx 1.68\ \mathrm{nm}$$

This is enormously broader than an ordinary narrow photospheric absorption line.

6.4 Why Such a Broad Component Can Be Difficult to Notice

A broad spectral component does not necessarily appear as a deep line.

If approximately the same integrated absorption is redistributed over a much larger wavelength interval, its average depth decreases.

For a simplified equal-area estimate,

$$d_0 w_0 = dW$$

where d_0 and w_0 are the depth and width of the narrow feature and d and W are the corresponding quantities after broad redistribution.

Therefore,

$$d = d_0 \frac{w_0}{W}$$

If a narrow feature has, for example,

$$w_0 = 0.02\ \mathrm{nm}$$

and the reconstructed broad component has

$$W = 1.68\ \mathrm{nm}$$

then

$$\frac{W}{w_0} \approx 84$$

A narrow feature with a depth of 50% would then correspond, in this very simplified equal-area illustration, to an average broad depression of only about

$$d \approx 0.6\backslash\%$$

The numerical example is not intended as a detailed radiative-transfer model. It only illustrates an important experimental point:

$$\text{large velocity width} \Rightarrow \text{deep broad spectral feature}$$

A very broad component can instead appear as a small variation of the local continuum or be partly removed by spectral normalization.

6.5 Narrow and Broad Spectral Components Can Coexist

The present interpretation therefore allows two spectral structures to coexist.

A relatively narrow component can reflect the spatial-wavelength structure measured directly by the FPI, while a much broader and shallower component can arise when the longitudinal interaction-frequency distribution is reconstructed by a diffraction grating.

Schematically,

$$\text{narrow FPI feature} + \text{broad shallow grating component}$$

need not represent two unrelated plasma populations.

They can be two instrumental representations of the same underlying velocity field.

6.6 Connection with Part VIII

Part VIII proposed a direct differential test using the same incoming astronomical beam in two states.

In the first state, the beam enters the Fabry–Pérot interferometer directly.

In the second, the beam first passes through the zero-order path of a diffraction grating and is then measured by the same interferometer.

The corresponding wavelengths are

$$\lambda_{\mathrm{dir}}$$

and

$$\lambda_{\mathrm{gr}}$$

Within the present model,

$$f = \frac{c}{\lambda_{\mathrm{gr}}}$$

and the propagation velocity of the direct astronomical radiation is obtained from

$$u = f\lambda_{\mathrm{dir}}$$

so that

$$\frac{u}{c} = \frac{\lambda_{\mathrm{dir}}}{\lambda_{\mathrm{gr}}}$$

This differential method avoids the need to know the absolute emitted wavelength of the astronomical source with the same precision.

The solar center-to-limb analysis presented here is not equivalent to that controlled experiment. It is instead a comparison with already existing observations.

6.7 Existing Solar Measurements as a Consistency Check

The existing solar data considered in this paper show two features that are qualitatively compatible with the Part VIII interpretation.

First, direct high-resolution spectral measurements display relatively small wavelength shifts when expressed through the conventional Doppler relation.

Second, the center-to-limb variation of those shifts leads, within the transverse model, to characteristic velocities of order

$$300 - 400 \text{ km s}^{-1}$$

The apparent contradiction between a small measured wavelength shift and a large inferred physical velocity is therefore exactly the type of distinction expected if spatial wavelength and interaction frequency are not altered in the same way by source motion.

6.8 Main Result

The comparison between Fabry–Pérot and diffraction-grating measurements provides the experimental bridge between Part VIII and the solar analysis of Part IX.

Within the present model:

$$\text{FPI} \rightarrow \text{direct spatial-wavelength response}$$

whereas

$$\text{grating} \rightarrow \text{frequency-dependent wavelength reconstruction}$$

A large longitudinal plasma-velocity distribution can therefore remain weakly expressed in an FPI wavelength measurement while becoming a broad wavelength distribution after grating reconstruction.

This resolves, within the proposed framework, why inferred collective velocities of several hundred kilometres per second need not appear as equally large conventional line shifts.

With this result, the first part of the paper is essentially complete. The spectral measurements point toward a characteristic collective plasma-velocity scale of several hundred kilometres per second.

The second part now asks a different question: **what does such a velocity scale imply for the physical state, energy exchange, and visible-light production of the solar photosphere?**

7. Collective Plasma Motion, Temperature, and Electron Energy

In the following discussion, the shorthand $v_{\text{plasma}} \sim 300 - 400 \text{ km s}^{-1}$ refers to the characteristic collective-flow velocity inferred from D under the assumption that the dominant photospheric motion is approximately vertical.

The velocity scale derived in the first part of this paper is much larger than the velocities usually associated with the quiet solar photosphere. If interpreted immediately as random thermal motion, values of several hundred kilometres per second would imply temperatures far above the conventional photospheric temperature.

That interpretation, however, is not necessary.

The central distinction is between collective plasma motion and microscopic random motion.

The velocity of a particle can be written as

$$v_i = U + \delta v_i$$

where U is the collective velocity of the local plasma flow and δv_i is the particle velocity relative to that flow.

The first quantity describes organized motion of the plasma structure. The second is associated with local thermal and microscopic motion.

7.1 Collective Velocity Is Not Temperature

A large collective velocity does not by itself imply a high thermodynamic temperature.

If all particles within a local plasma element move approximately together,

$$|\delta v_i| \ll |U|$$

then the plasma can possess a large translational kinetic energy as a whole while

maintaining comparatively small internal random velocities.

The kinetic energy of one particle is

$$E_k = \frac{1}{2} m v^2$$

but the temperature of the plasma is related primarily to the distribution of the random component δv_i, not directly to the collective component U.

Thus,

$$|U| \sim 300 - 400 \text{ km s}^{-1}$$

does not automatically imply that the local plasma temperature corresponds to a Maxwellian distribution with the same characteristic particle speed.

This distinction is essential for the present interpretation.

7.2 The Same Velocity Gives Very Different Particle Energies

At the same velocity, particle kinetic energy is proportional to mass.

For an electron,

$$E_{k,e} = \frac{1}{2} m_e v^2$$

while for a proton,

$$E_{k,p} = \frac{1}{2} m_p v^2$$

Therefore,

$$\frac{E_{k,e}}{E_{k,p}} = \frac{m_e}{m_p} \approx \frac{1}{1836}$$

At

$$v = 300 \text{ km s}^{-1}$$

the electron kinetic energy is approximately

$$E_{k,e} \approx 0.26 \text{ eV}$$

while the proton kinetic energy is approximately

$$E_{k,p} \approx 470 \text{ eV}$$

At

$$v = 400 \text{ km s}^{-1}$$

the corresponding values are approximately

$$E_{k,e} \approx 0.46 \text{ eV}$$

and

$$E_{k,p} \approx 835 \text{ eV}$$

Thus, the same collective plasma velocity can represent a substantial kinetic-energy reservoir in heavy particles while electrons moving with the flow remain comparatively low-energy particles.

7.3 Why This Distinction Matters

This difference is important for the interpretation of photospheric radiation.

A plasma flow moving at several hundred kilometres per second can contain:

$$\text{large collective kinetic energy}$$

while simultaneously maintaining

$$\text{low electron kinetic energy relative to the local flow}$$

The low electron mass therefore allows a dynamically energetic plasma to coexist with electrons that remain suitable for low-energy interactions with atoms and ions.

The plasma can consequently be both dynamically active and radiatively efficient without requiring all electrons to belong to a high-energy population.

7.4 Relative Velocity Between Neighboring Plasma Flows

The important quantity for microscopic interactions is often not the absolute collective velocity of one flow, but the relative velocity between neighboring flows.

If two plasma structures move with collective velocities

$$U_1$$

and

$$U_2$$

their relative velocity is

$$\Delta U = U_1 - U_2$$

An electron passing from one flow into another can therefore enter the new plasma environment with an approximate relative velocity

$$ve,\mathrm{rl} \approx \Delta U$$

and corresponding kinetic energy

$$E_{e,\mathrm{rel}} = \frac{1}{2} m_e |\Delta U|^2$$

For a relative velocity of

$$|\Delta U| = 300\ \mathrm{km\ s^{-1}}$$

the electron energy is again only about

$$E_{e,\mathrm{rel}} \approx 0.26\ \mathrm{eV}$$

while for

$$|\Delta U| = 400\ \mathrm{km\ s^{-1}}$$

it is about

$$E_{e,\mathrm{rel}} \approx 0.46\ \mathrm{eV}$$

Even large plasma-flow differences can therefore correspond to relatively small electron energies.

7.5 Plasma Boundaries as Energy-Conversion Regions

The small electron energy does not mean that the plasma-flow interaction is weak.

The total energy density of the flow can be large because ions and heavier particles carry most of the translational kinetic energy.

At boundaries between neighboring flows, velocity differences can produce shear, mixing, turbulence, electric fields, magnetic fluctuations, and collisions.

The energy-conversion sequence can be represented schematically as

$$\begin{aligned} &\text{collective kinetic energy} \\ &\rightarrow \text{shear and turbulence} \\ &\rightarrow \text{microscopic particle energy} \end{aligned}$$

Part of the ordered energy of the plasma can therefore be redistributed into ionization, excitation, electron release, capture, and radiation.

The boundary should not automatically be described as having a high temperature. More precisely, it contains a large reservoir of ordered relative kinetic energy that can become heat only after it is randomized.

7.6 Electron Energy and Visible-Light Production

The electron energies associated directly with several hundred kilometres per second are small enough to be important for capture and recombination processes.

For example,

$$E_{k,e} \sim 0.1 - 1\ \mathrm{eV}$$

is much smaller than the ground-state ionization energy of hydrogen, but it is comparable with the binding energies of higher atomic levels.

For hydrogen,

$$E_n = -\frac{13.6}{n^2}\ \mathrm{eV}$$

so that

$$|E_3| = 1.51\ \mathrm{eV}$$

$$|E_4| = 0.85\ \mathrm{eV}$$

and

$$|E_5| = 0.54\ \mathrm{eV}$$

This makes low-energy electron capture into higher excited states physically relevant.

The importance of the velocity scale obtained from the spectral analysis is therefore not that it uniquely determines the energy of a visible photon.

Rather, it places the plasma in a regime where low-energy electron interactions can coexist with a large reservoir of collective kinetic energy.

7.7 Comparison with Much Smaller Plasma Velocities

If the characteristic collective velocities were only a few kilometres per second, the kinetic-energy density and the energy available in collisions between neighboring flows would be much smaller.

Because kinetic energy scales as

$$E_k \propto v^2$$

reducing a characteristic velocity from

$$300\ \mathrm{km\,s^{-1}}$$

to

$$3\ \mathrm{km\,s^{-1}}$$

reduces the kinetic energy per particle at the same mass by a factor of

$$\left(\frac{3}{300}\right)^2 = 10^{-4}$$

The corresponding capacity for shear-driven mixing, turbulence, ionization, repeated electron exchange, and other microscopic processes would therefore be strongly reduced.

This does not mean that visible light cannot be produced at low plasma velocities.

It means that the rate of energy redistribution and the number of radiative microscopic events can be much more limited.

7.8 Main Physical Consequence

The velocity scale derived from the spectral measurements therefore has two simultaneous consequences.

First,

$$v_{\mathrm{plasma}} \sim 300 - 400\ \mathrm{km\,s^{-1}}$$

implies a large reservoir of collective kinetic energy.

Second, because of the small electron mass,

$$E_{k,e} \sim 0.3 - 0.5\ \mathrm{eV}$$

for electrons moving with the same characteristic velocity.

This combination is especially interesting:

$$\text{large plasma energy reservoir} + \text{low-energy electrons}$$

It provides a natural basis for a highly dynamic photosphere in which strong mixing and energy transfer can coexist with frequent low-energy electron capture and radiative transitions.

The next section examines these microscopic processes directly and considers how turbulence, electron capture, recombination, and repeated transitions can contribute to the strong visible radiation of the photosphere.

8. Electron Capture, Turbulence, and Visible-Light Production

The preceding section showed that collective plasma velocities of several hundred kilometres per second can coexist with comparatively low electron kinetic energies. This combination is important because visible radiation does not require every electron to be highly energetic.

The decisive quantity is instead the rate at which electrons are released, transported, captured, excited, and returned to bound states.

A highly dynamic plasma can therefore produce strong visible radiation through a large number of moderate-energy microscopic events.

8.1 Electron Capture into an Ion

A free electron entering the Coulomb field of a positive ion is accelerated toward the ion.

However, Coulomb attraction alone does not guarantee capture. The electron must lose sufficient energy and momentum to become bound.

One possible process is radiative recombination:

$$A^{q+} + e^- \rightarrow A^{(q-1)+*} + \gamma$$

Another possibility in a sufficiently dense plasma is three-body recombination:

$$A^{q+} + e^- + e^- \rightarrow A^{(q-1)+*} + e^-$$

The newly formed atom or ion can remain in an excited state and subsequently undergo further radiative transitions.

The capture probability depends on the ion, electron energy, plasma density, and available interaction channels. A low-energy electron is therefore not automatically captured, but low relative energy can make capture into weakly bound states physically favorable.

8.2 Capture into Excited States

For hydrogen-like levels,

$$E_n = -\frac{13.6}{n^2}\ \text{eV}$$

Higher levels are only weakly bound.

For example,

$$|E_3| = 1.51\ \text{eV}$$

$$|E_4| = 0.85\ \text{eV}$$

$$|E_5| = 0.54\ \text{eV}$$

These energies are comparable with the kinetic energies of electrons associated with relative plasma velocities of several hundred kilometres per second.

For radiative capture into level n,

$$E_\gamma = E_{k,e} + \frac{13.6}{n^2}\ \text{eV}$$

The emitted photon therefore contains both the kinetic energy of the incoming electron and the binding energy released during capture.

8.3 Visible Photons from Low-Energy Electrons

An electron does not need to possess several electronvolts of kinetic energy in order to participate in the production of a visible photon.

For example, if

$$E_{k,e} = 0.46\ \text{eV}$$

and the electron is radiatively captured into the hydrogen level

n = 3

then

$$E_\gamma = 0.46 + \frac{13.6}{9} \approx 1.97\ \text{eV}$$

which lies in the visible range.

This is an illustrative example rather than a claim that capture preferentially occurs into n=3.

The important point is that visible radiation can arise from low-energy electrons because part of the photon energy comes from the binding energy of the atom or ion.

8.4 Radiative Cascades

Capture into an excited state can be followed by a sequence of downward transitions.

Schematically,

$$n_{\text{high}} \rightarrow n_1 \rightarrow n_2 \rightarrow \cdots \rightarrow n_{\text{low}}$$

Each transition can emit a photon with energy

$$E_{\gamma,ij} = E_i - E_j$$

A single capture event can therefore initiate several radiative transitions.

The resulting photons may appear in different parts of the spectrum, including the visible range.

The total photospheric radiation can thus result from the superposition of an enormous number of individual capture and cascade events.

8.5 Continuous Electron Recycling

The process does not end when the electron reaches a bound state.

Subsequent collisions, electromagnetic interactions, or local heating can ionize the atom again:

$$A + E_{\mathrm{in}} \rightarrow A^{+} + e^{-}$$

The electron can then enter another local plasma environment and participate in a new capture event.

The microscopic cycle can therefore be represented as

$$\begin{aligned} &\text{ionization} \rightarrow \text{free electron} \rightarrow \text{transport} \\ &\qquad \rightarrow \text{capture} \\ &\qquad \rightarrow \text{radiative transitions} \\ &\qquad \rightarrow \text{ionization} \end{aligned}$$

The same electron may participate in this cycle repeatedly.

Photospheric luminosity is therefore determined less by the energy history of one electron than by the total number of such cycles occurring per unit time.

8.6 Role of Turbulence and Mixing

This is where large collective plasma velocities become especially important.

Neighboring flows with different collective velocities contain a reservoir of relative kinetic energy:

$$\Delta U = U_1 - U_2$$

At their boundaries, this energy can drive shear, turbulence, mixing, electric fields, magnetic fluctuations, and collisions.

These processes can increase the rate of:

$$\text{electron release}$$

$$\text{particle transport}$$

$$\text{ionization and excitation}$$

and

$$\text{capture and recombination}$$

The importance of turbulence is therefore not that it must raise all electrons to very high energies.

Its more general role is to increase the frequency with which particles move between different microscopic states and environments.

8.7 Event Rate as the Main Link to Brightness

The visible radiative power can be expressed schematically as

$$P_{\mathrm{vis}} \sim R_{\mathrm{events}} \overline{E_{\gamma}}$$

where R_{events} represents the rate of microscopic processes that produce visible photons.

The photon energy may remain of order only a few electronvolts, while the total power becomes large because

$$R_{\mathrm{events}}$$

is very large.

This provides a direct link between plasma dynamics and luminosity:

$$\begin{aligned} &\text{large flow velocities} \\ &\qquad \rightarrow \text{stronger shear and mixing} \\ &\qquad \rightarrow \text{larger } R_{\mathrm{events}} \\ &\qquad \rightarrow \text{stronger radiation} \end{aligned}$$

The precise dependence need not be linear.

The important point is that increasing the dynamical activity of the plasma increases the opportunities for ionization, transport, capture, recombination, and radiative transition.

8.8 Why Small Plasma Velocities Would Limit the Process

If neighboring flows differed by only a few kilometres per second, their relative kinetic-energy reservoir would be much smaller.

Since kinetic energy scales as

$$E_k \propto v^2$$

the energy available for turbulence and mixing decreases rapidly with velocity.

A reduction from

$$300\ \mathrm{km\,s^{-1}}$$

to

$$3\ \mathrm{km\,s^{-1}}$$

corresponds to a factor of

$$10^{-4}$$

in kinetic energy per particle of the same mass.

Visible radiation could still be produced, but the rate of repeated microscopic interactions would be expected to be much more limited.

Thus, large plasma velocities are favorable not because they uniquely determine the photon energy, but because they sustain a much more active cycle of particle exchange and radiation.

8.9 A Dynamical Picture of the Photosphere

The emerging picture is therefore one of a continuously interacting plasma.

Inside a local flow, particles may share approximately the same collective velocity.

At interfaces between flows, differences in collective velocity generate turbulence and mixing.

These boundary regions can redistribute kinetic energy into microscopic particle processes.

Electrons are repeatedly released, transported, captured, and re-emitted into the plasma.

The resulting chain can be summarized as

$$\begin{aligned}&\text{collective plasma motion}\\ &\quad\rightarrow \text{turbulence and mixing}\\ &\quad\rightarrow \text{electron exchange}\\ &\quad\rightarrow \text{capture and cascades}\\ &\quad\rightarrow \text{visible radiation}\end{aligned}$$

The strong visible emission of the photosphere can therefore be associated with a high rate of repeated microscopic events sustained by a dynamically active plasma.

8.10 Main Result

Visible-light production is not restricted to either very slow or very fast electrons.

Low-energy electrons can participate efficiently in capture and recombination processes, while more energetic electrons contribute to excitation, ionization, and additional radiative channels.

The importance of the velocity scale

$$v_{\mathrm{plasma}} \sim 300 - 400\ \mathrm{km\,s^{-1}}$$

lies primarily in the large dynamical activity that such flows can support.

Within the present interpretation,

$$\text{high plasma velocity} \rightarrow \text{high interaction rate}$$

and therefore potentially

$$\begin{aligned}&\text{high interaction rate}\\ &\quad\rightarrow \text{high visible luminosity}\end{aligned}$$

This provides the second major result of Part IX: the velocity scale inferred independently from the spectral measurements is also a velocity scale capable of sustaining an intensely dynamic and radiatively active photosphere.

9. Discussion

The results of this paper can be reduced to two connected conclusions.

The first concerns measurement. Existing center-to-limb spectral shifts are small when expressed through the conventional first-order Doppler relation. Within the interpretation developed in Part VIII and applied here, however, the same measurements correspond to a characteristic anisotropic velocity scale of several hundred kilometres per second.

For predominantly vertical plasma flows,

$$D = \sqrt{\sigma_z^2 - \sigma_h^2} \approx \sigma_z$$

and the measurements considered here give approximately

$$D \sim 300 - 400\ \mathrm{km\,s^{-1}}$$

This result appears across several photospheric spectral lines and therefore does not depend on one single atomic transition.

9.1 From Spectral Shift to Collective Plasma Motion

The main observational result is not that the photospheric plasma is directly measured to move at 300–400 km/s.

Rather, the measured wavelength changes correspond, within the transverse-wavelength interpretation, to an anisotropic velocity scale of this magnitude.

The physical interpretation becomes especially simple if the dominant flows are approximately vertical:

$$\sigma_h \ll \sigma_z$$

so that

$$D \approx \sigma_z$$

and D becomes an estimate of the characteristic vertical collective-flow velocity.

The distinction between the measured wavelength displacement and the inferred plasma velocity therefore remains essential throughout the analysis.

9.2 Why Large Collective Velocity Need Not Mean High Temperature

The second part of the paper concerns the physical meaning of such velocities.

The particle velocity is separated into collective and microscopic components:

$$v_i = U + \delta v_i$$

A large collective velocity U does not by itself imply a large random velocity δv_i, and therefore does not directly determine the thermodynamic temperature.

This allows a photospheric flow to contain a large reservoir of collective kinetic energy while electrons remain in a comparatively low-energy microscopic regime.

The important consequence is that large-scale plasma dynamics and low-energy electron capture are not mutually exclusive.

9.3 Velocity as a Driver of Radiative Activity

Visible radiation is not restricted to one particular electron velocity.

Low-energy electrons can participate in radiative capture and recombination, while more energetic particles can contribute to excitation, ionization, and additional radiative channels.

The visible power is therefore better represented schematically as

$$P_{\mathrm{vis}} \sim R_{\mathrm{events}}\overline{E_\gamma}$$

where R_{events} is the total rate of microscopic processes producing visible photons.

The main importance of large collective plasma velocities is therefore dynamical.

Large relative velocities between neighboring flows can increase shear, turbulence, mixing, particle transport, ionization, capture, and recombination.

The proposed chain is

large collective velocity
→ strong plasma dynamics
→ large microscopic event rate
→ strong visible radiation

The velocity does not uniquely determine the photon energy. It increases the capacity of the plasma to sustain repeated energy-transfer and radiative processes.

9.4 Convergence of the Two Parts of the Paper

The central result of Part IX is therefore the convergence of two arguments.

From the measurement side:

$$\text{center-to-limb spectral measurements} \rightarrow D \sim 300 - 400\ \mathrm{km\,s^{-1}}$$

From the physical side:

$$300 - 400\ \mathrm{km\,s^{-1}} \rightarrow \text{strong plasma dynamics and high radiative activity}$$

The two arguments do not prove each other.

Their significance is that the velocity scale inferred from the proposed interpretation of the measurements is also physically compatible with a dynamically active and strongly radiating photosphere.

The present analysis remains conceptual. A complete quantitative model would still require the detailed velocity distribution, flow geometry, density, turbulence, electron-capture and ionization rates, and radiative-transfer calculation.

The controlled Fabry–Pérot versus diffraction-grating experiment proposed in Part VIII therefore remains the direct experimental test of the underlying measurement interpretation.

10. Conclusions

Part IX has examined whether the measurement principles developed in Part VIII can be connected with the physical state of the solar photosphere.

Within the present interpretation, center-to-limb wavelength changes are associated with a transverse-motion contribution. Several photospheric spectral lines lead to a characteristic anisotropic velocity scale of approximately

$$D \sim 300 - 400\ \mathrm{km\,s^{-1}}$$

For predominantly vertical plasma flows,

$$D \approx \sigma_z$$

so this scale can be interpreted as an estimate of the characteristic vertical collective-flow velocity.

Such velocities need not correspond to random thermal motion. The particle velocity can be separated as

$$v_i = U + \delta v_i$$

allowing large collective motion to coexist with much smaller microscopic velocities.

This distinction is important for photospheric radiation. Visible photons can be produced over a broad range of electron energies through capture, recombination, excitation, and radiative cascades. The principal role of large collective velocities is therefore not to determine one characteristic photon energy, but to increase the dynamical activity of the plasma and the rate of microscopic radiative events.

The two main results of the paper can therefore be summarized as

$$\text{spectral measurements} \rightarrow D \sim 300 - 400\ \mathrm{km\,s^{-1}}$$

and

$$\text{large collective velocity} \rightarrow \text{strong plasma dynamics} \rightarrow \text{high radiative event rate}$$

The same velocity scale thus appears both in the interpretation of the measurements and in the proposed physical mechanism for sustaining strong visible photospheric radiation.

This agreement does not yet constitute a complete quantitative model of the photosphere. It does, however, provide a coherent connection between the measurement method of Part VIII, the inferred collective plasma motion, and the strong visible emission of the solar photosphere.

References

(1) Cavallini, F. (2006). *IBIS: A New Post-Focus Instrument for Solar Imaging Spectroscopy*. **Solar Physics, 236**, 415–439. https://doi.org/10.1007/s11207-006-0103-8. Springer Nature Link

(2) Janssen, K., & Cauzzi, G. (2006). *Dynamics of the Solar Photosphere with IBIS. I. Reversed Intensity Structure in the Mid-Photosphere*. **Astronomy & Astrophysics, 450**, 365–374. https://doi.org/10.1051/0004-6361:20054310. aanda.org

(3) Kramida, A., Ralchenko, Yu., Reader, J., & NIST ASD Team (2024). *NIST Atomic Spectra Database, Version 5.12*. National Institute of Standards and Technology, Gaithersburg, MD. https://doi.org/10.18434/T4W30F. NIST

(4) Löhner-Böttcher, J., Schmidt, W., Stief, F., Steinmetz, T., & Holzwarth, R. (2018). *Convective Blueshifts in the Solar Atmosphere. I. Absolute Measurements with LARS of the Spectral Lines at 6302 Å*. **Astronomy & Astrophysics, 611**, A4. https://doi.org/10.1051/0004-6361/201732107. ResearchGate

(5) Löhner-Böttcher, J., Schmidt, W., Schlichenmaier, R., Steinmetz, T., & Holzwarth, R. (2019). *Convective Blueshifts in the Solar Atmosphere. III. High-Accuracy Observations of Spectral Lines in the Visible*. **Astronomy & Astrophysics, 624**, A57. https://doi.org/10.1051/0004-6361/201834925. aanda.org

(6) Nordlund, Å., Stein, R. F., & Asplund, M. (2009). *Solar Surface Convection*. **Living Reviews in Solar Physics, 6**, 2. https://doi.org/10.12942/lrsp-2009-2. Springer Nature Link

(7) Prša, A., Harmanec, P., Torres, G., Mamajek, E., Asplund, M., Capitaine, N., Christensen-Dalsgaard, J., et al. (2016). *Nominal Values for Selected Solar and Planetary Quantities: IAU 2015 Resolution B3*. **The Astronomical Journal, 152**, 41. https://doi.org/10.3847/0004-6256/152/2/41. research.si.edu

(8) Reardon, K. P., & Cavallini, F. (2008). *Characterization of Fabry–Pérot Interferometers and Multi-Etalon Transmission Profiles: The IBIS Instrumental Profile*. **Astronomy & Astrophysics, 481**, 897–912. https://doi.org/10.1051/0004-6361:20078473. aanda.org

(9) Rutten, R. J. (2003). *Radiative Transfer in Stellar Atmospheres*. Utrecht University Lecture Notes, 8th ed.

(10) Vernazza, J. E., Avrett, E. H., & Loeser, R. (1981). *Structure of the Solar Chromosphere. III. Models of the EUV Brightness Components of the Quiet Sun*. **The Astrophysical Journal Supplement Series, 45**, 635–725. https://doi.org/10.1086/190731.